A mid to late Holocene cryptotephra framework from eastern North America

Mackay, H., Hughes, P. D. M., Jensen, B. J. L., Langdon, P. G., Pyne-O'Donnell, S. D. F., Plunkett, G., Froese, D. G., Coulter, S., & Gardner, J. E. (2016). A mid to late Holocene cryptotephra framework from eastern North America. *Quaternary Science Reviews*, *132*, 101-113. https://doi.org/10.1016/j.quascirev.2015.11.011

Published in:
Quaternary Science Reviews

Document Version:
Publisher's PDF, also known as Version of record

Queen's University Belfast - Research Portal:
Link to publication record in Queen's University Belfast Research Portal

Quaternary Science Reviews 132 (2016) 101–113

Contents lists available at ScienceDirect

Quaternary Science Reviews

journal homepage: www.elsevier.com/locate/quascirev

A mid to late Holocene cryptotephra framework from eastern North America

Helen Mackay [a, *], Paul D.M. Hughes [a], Britta J.L. Jensen [b, 1], Pete G. Langdon [a], Sean D.F. Pyne-O'Donnell [b], Gill Plunkett [b], Duane G. Froese [c], Sarah Coulter [d], James E. Gardner [e]

[a] Geography and Environment, University of Southampton, Southampton, SO17 1BJ, UK
[b] School of Geography, Archaeology and Palaeoecology, Queen's University Belfast, Belfast, BT7 1NN, UK
[c] Department of Earth and Atmospheric Sciences, University of Alberta, Edmonton, AB, T6G 2E3, Canada
[d] Omagh Minerals Ltd, 56 Botera Upper Rd., Omagh, BT78 5LH, UK
[e] Department of Geological Sciences, Jackson School of Geosciences, The University of Texas at Austin, TX, 78705, USA

ARTICLE INFO

Article history:
Received 18 August 2015
Received in revised form
29 October 2015
Accepted 14 November 2015
Available online 10 December 2015

Keywords:
Tephra
Cryptotephra
Volcanic ash
Peatlands
Late Holocene
North America

ABSTRACT

Holocene cryptotephras of Alaskan and Pacific Northwestern origin have recently been detected *ca.* 7000 km away on the east coast of North America. This study extends the emerging North American tephrochronological framework by geochemically characterising seventeen cryptotephra layers from four newly explored peatlands. All detected tephras were deposited during the late Holocene, with no horizons present in the peat between *ca.* 3000–5000 years ago. The prevalence of the Alaskan White River Ash eastern lobe (AD 847 ± 1) is confirmed across the eastern seaboard from Newfoundland to Maine and a regional depositional pattern from Mount St Helens Set W (AD 1479–1482) is presented. The first occurrences of four additional cryptotephras in eastern North America are described, three of which may originate from source regions in Mexico, Kamchatka (Russia) and Hokkaido (Japan). The possibility of such tephras reaching eastern North America presents the opportunity to link palaeo-archives from the tropics and eastern Asia with those from the western Atlantic seaboard, aiding inter-regional comparisons of proxy-climatic records.

1. Introduction

Precise palaeoclimatic comparisons between sites and regions are essential for understanding past climate dynamics. However, inter-site correlation is often limited by poor chronological control. Tephrochronology provides an age-equivalent dating method by using volcanic ash layers with unique geochemical signatures as time-specific marker horizons (isochrons) to connect and synchronise archives (e.g. Alloway et al., 2013; Lowe, 2011). These isochrons are used to create high-resolution records of palaeoenvironmental or archaeological events, the relative timing of which can be compared across sites and regions (e.g. Hall et al., 1993; Lane et al., 2013a, b; Lowe et al., 2012; Plunkett and Swindles, 2008). An air-fall ash layer from a volcanic eruption can be regarded as having been deposited instantaneously in geological time and can thus adopt the eruption's age wherever it is found as a well-defined primary horizon. If the eruption history is unknown or poorly constrained then archives can still be correlated if the same tephra horizons are present and these fixed tie-points can be used to create a common timescale (Lowe, 2011).

Investigations of far-travelled microscopic volcanic glass shards (cryptotephra – with dimensions typically <~125 μm; *sensu* Lowe and Hunt, 2001) in sediments allow for the detection of previously unrecognised ash horizons and sometimes unknown eruptions. These cryptotephras provide the opportunity to obtain precise chronologies in areas that were thought to be outside the range of tephrochronology, thus greatly expanding the dating framework and increasing the number of regions that can be linked together. Cryptotephra studies originally focused on Icelandic tephras in Western Europe, but the potential for North American cryptotephra studies is rapidly emerging (Payne et al., 2008; Pyne-

* Corresponding author. School of Geography, Politics and Sociology, University of Newcastle, Newcastle upon Tyne, NE1 7RU, UK.
E-mail address: Helen.Mackay@newcastle.ac.uk (H. Mackay).
[1] Current address: Royal Alberta Museum, Edmonton, AB, T5N 0M6, Canada.

http://dx.doi.org/10.1016/j.quascirev.2015.11.011

O'Donnell et al., 2012).

The first crypto-tephrostratigraphy for the eastern seaboard of North America in Newfoundland was recently developed from one peatland, Nordan's Pond Bog (Pyne-O'Donnell et al., 2012). Seven tephras in this *ca.* 9000-yr-long sequence were correlated to sources in Alaska and the Cascade Range, four of which occurred during the late Holocene: tephra from Mount St Helens (MSH) set W, AD 1479–1482 (Fiacco et al., 1993; Yamaguchi, 1985; Yamaguchi and Hoblitt, 1995); White River Ash, eastern lobe (WRAe), ~AD 847 ± 1 (Jensen et al., 2014a); Newberry Pumice *ca.* 1460 cal yr BP (Kuehn and Foit, 2006); and Aniakchak, Greenland Ice Core Chronology (GICC05) age 3590 ± 1 BP (Coulter et al., 2012). A fifth late Holocene tephra was tentatively correlated with Mount Augustine G, *ca.* 2100 cal yr BP (Tappen et al., 2009). However, subsequent geochemical comparisons with reference materials suggest that although this tephra shares characteristics with material sourced from Augustine, it is unlikely to be Augustine G (Kristi Wallace, pers. comm.). All correlated tephras in Nordan's Pond Bog were of North American origin but the detection of horizons from other source regions cannot be precluded. Ash from the 2010 eruption of Eyjafjallajökull, Iceland, approached Newfoundland (Davies et al., 2010) and tephra from Changbaishan, China, has been identified in Greenland ice cores (Sun et al., 2013); therefore, sources even further afield cannot be discounted.

This study builds on the existing eastern seaboard record by contributing four newly developed peatland tephrostratigraphies from the region. Undisturbed peatlands are excellent archives for preserving tephrostratigraphies since cryptotephra horizons are often present in discrete layers that have been subjected to minimal post-depositional movement (Dugmore and Newton, 1992; Dugmore et al., 1996; Payne et al., 2005). The primary air-fall tephra deposit may be reworked in some peatlands, particularly if the site has been disturbed (e.g. Swindles et al., 2013). However, the majority of deposited shards are usually confined within a narrow stratigraphic layer of no more than a few centimetres depth (Swindles and Plunkett, 2011). The findings from this study extend the known regional spatial distribution of previously identified tephras, add several newly characterised tephras, and demonstrate the increased potential of this technique in obtaining late Holocene high-precision chronologies. The major and minor element chemistry of several newly characterised tephras in this study suggests that there is potential for delivery of tephra from more distal, and previously unconsidered source regions, to eastern North America.

2. Methods

The study sites, Saco Heath (SCH10: 43°33′05″ N; 70°2′03″ W), Villagedale Bog (VDB12: 43°31′09″ N; 65°31′54″ W), Framboise Bog (FBB12: 45°43′14: N; 60°33′09″ W) and Jeffrey's Bog (JRB12: 48°12′46″ N; 58°49′06″ W) are ombrotrophic plateau bogs located along a south-west to north-east transect across Maine, Nova Scotia, and Newfoundland (Fig. 1). The cores were sampled from the centre of each bog using an 11-cm-diameter Russian pattern corer, following a full stratigraphic investigation based on the Troels-Smith (1955) system.

The stratigraphic position and shard concentration of the cryptotephra layers were established by the standard method of ashing the peat at 5 cm contiguous intervals (Pilcher and Hall, 1992). The ashed residues were mounted in glycerol and counted under a high power microscope. Guided by these counts, the stratigraphic depth of cryptotephra layers were refined to 1 cm resolution. Samples containing less than fifteen shards in the 5 cm resolution counts were not investigated further since they were unlikely to yield sufficient shard concentrations to be comprehensively geochemically characterised. If two consecutive samples contained similar elevated concentrations of cryptotephra shards then both were investigated at 1 cm resolution. Depths containing a further local rise in shard concentration within sections of successive elevated cryptotephra concentrations were also analysed at 1 cm resolution. Samples containing peak tephra concentrations were selected for geochemical analysis (Fig. 2; Appendix A, Supplementary Information), based on the assumption that they are representative of the primary air-fall deposition (cf. Payne and Gehrels, 2010).

Glass shards for electron probe microanalyses were extracted from the peat matrix using the heavy liquid flotation method (Blockley et al., 2005), modified with additional cleaning floats and gentle stirring to improve shard extraction yields. The flotation method was chosen to avoid any possible chemical alteration that may arise from the alternative acid digestion technique (Blockley et al., 2005). Whilst other peat studies have obtained consistent results using acid digestion (e.g. Roland et al., 2015), flotation was deemed an important precaution since the shards were small with a high surface to volume ratio, characteristics which may make shards prone to chemical alteration (Blockley et al., 2005; Dugmore et al., 1992). Extracted shards were mounted on epoxy resin discs and exposed at the surface by careful grinding and polishing.

Major and minor element compositions of single glass shards of unknown cryptotephra horizons were determined by electron probe microanalysis (EPMA) with wavelength dispersive spectrometry (WDS-EPMA) at the Tephra Analytical Unit, University of Edinburgh, using a 3 μm beam (Appendix B.1, Supplementary Information). This beam size was used because shard sizes were typically very small (25–102.5 μm) with many vesicles (Hayward, 2012). Ksudach 1 (KS1) proximal tephras were analysed at the University of Edinburgh using the same parameters and at Queen's University Belfast (analytical set up outlined in Appendix B.2, Supplementary Information). All Mount St. Helen's, Jala Pumice and White River Ash glass analyses were analysed at the University of Alberta on a JEOL 8900 using a 10 μm beam, 6 nA current, and 15 keV voltage. Analyses at all laboratories used a similar suite of minerals and glass for calibration, and a Lipari obsidian as a secondary standard to track the quality of calibration and assure repeatable analyses (e.g. Kuehn et al., 2011). The results of the standard analyses were consistent, predominantly remaining within the accepted analytical range (Appendix B, Supplementary Information). Therefore, the datasets are comparable among laboratories. All results are normalised to 100% on a water and volatile free basis (e.g. Froggatt, 1983; Lowe, 2011) to further assist comparisons. Correlations were identified by searching the University of Alberta tephra database (containing North American geochemical data with some Russian and Icelandic data), the Queen's University Belfast dataset (containing Icelandic and Russian geochemical data), Tephrabase (Newton et al., 1997; containing Icelandic/Europe and Mexican geochemical data) and published literature. Potential correlations to the unknown cryptotephra layers were visually examined using biplots of selected elements, with correlation strengths indicated by similarity coefficients (Borchardt et al., 1972; Appendix C, Supplementary Information).

Age-depth models were constructed using ^{14}C measurements on *Sphagnum* stems with the exception of the basal dates, which were obtained from bulk peat or brown mosses (Appendix D, Supplementary Information). ^{14}C measurements were converted to calendar age distributions using the IntCal13 calibration curve (Reimer et al., 2013) and the weighted averages of the date range distribution (2σ) are referred to throughout. Bayesian age-depth models were constructed using the R package "BACON" (Blaauw and Christen, 2011) assuming piece-wise linear accumulation (Fig. 2; Appendix D, Supplementary Information). The age-depth models were constructed using BACON's default prior settings

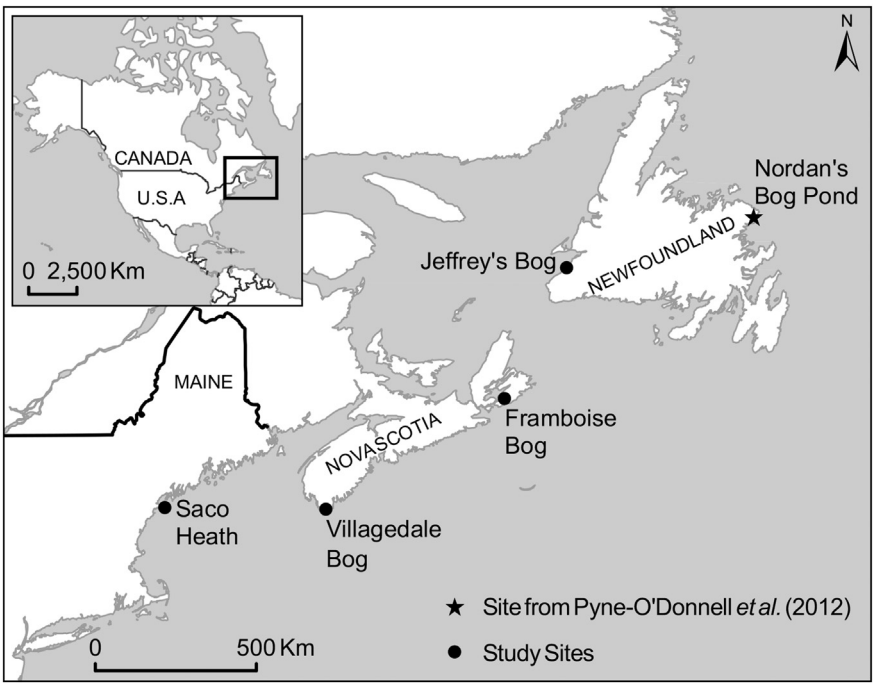

Fig. 1. The location of study sites Saco Heath (SCH10), Villagedale Bog (VDB12), Framboise Bog (FBB12) and Jeffrey's Bog (JRB12) in relation to the previous Newfoundland record from Nordan's Pond Bog (Pyne-O'Donnell et al., 2012).

(based on Goring et al., 2012), with the exception of the accumulation mean which was reduced to 10 years cm^{-1} to reflect average accumulation rates of oceanic raised peatlands.

3. Results and discussion

Cryptotephras extracted from seventeen layers across the four peat cores were geochemically analysed (Fig. 2), with all isolated horizons lying within the upper 2 m of peat. Attempts were made to geochemically characterise other layers of tephra containing *ca.* 15–20 shards/5 cm^3; however, too few shards were successfully isolated from the peat matrix despite using large volumes of peat (up to 10 cm^3). These cores may therefore contain more low concentration cryptotephra horizons that have not been characterised within this study. Background shard concentrations are generally low throughout the cores (average shards/5 cm^3: SCH10 = 1; VDB12 = 3.5; FBB12 = 2.6; JRB12 = 3).

Each crypto-tephrostratigraphy contains one prominent eruption occurring at 118 cm, 100 cm, 70 cm and 131 cm from the westernmost to easternmost sites, respectively. The glass compositions are rhyolitic, with some dacitic shards present in SCH10-42 and VDB12-42 (Appendix E, Supplementary Information). Each peak appears to represent a geochemically discrete tephra, with the exception of SCH10-42, which consists of two populations. As described below, eight of the cryptotephras investigated correlate with two known eruptions, four have possible correlations (FBB12-31, FBB12-162, VDB12-90, VDB12-176) and five have not been correlated with known late Holocene eruptions from North America, Iceland, Mexico, Kamchatka or Japan on account of geochemical differences or insufficient geochemical data (SCH10-42, SCH10-57, VDB12-42, VDB12-53, FBB12-47; Tables 1 and 2). All potential correlations are supported by core chronologies, major element geochemistry and shard morphology where reference material was available.

3.1. Correlated eruptions

3.1.1. Mount St Helens (MSH)

JRB12-71 (AD 1404–1578) correlates to the MSH set W eruptions of AD 1479 (MSH-Wn) to 1482 (MSH-We) (Fig. 3). The tephra is characterised by colourless pumiceous shards, similar to proximal samples of Mount St. Helens W. Distinguishing between the dominant ash layers from this set, Wn (which extended northeastwards) and We (which extended eastwards), is difficult because of the chemical similarities and short time interval between these ash layers (*ca.* 2–3 years; Fiacco et al., 1993; Mullineaux, 1996; Yamaguchi, 1985). However, when plotting JRB12-71 with proximal data from both eruptions, this tephra demonstrates a clear affinity with the We layer (Fig. 3). This is consistent with conclusions from Nordan's Pond Bog (Pyne-O'Donnell et al., 2012). The MSH set W ash is restricted to the northern study site, a pattern that could either be indicative of a patchy tephra fall-out distribution (e.g. Davies et al., 2010) or it may show that the southernmost limit of detectable cryptotephra deposition for this eruption lies close to Newfoundland. Analyses from further sites will be required to distinguish between these two possibilities.

3.1.2. The White River Ash (WRA)

All four sites contain horizons of highly pumiceous shards that geochemically correlate with the eastern lobe of the WRA (WRAe) from Mount Bona-Churchill, Alaska (Jensen et al., 2014a; Fig. 4; Appendix C.2, Supplementary Information). This tephra has been recently correlated to the European cryptotephra, "AD860B" (Jensen et al., 2014a) which has been dated by GICC05 to AD 847 ± 1 (Coulter et al., 2012). Three tephra layers characterised within SCH10 and two characterised within FBB12 geochemically correlate with the WRA (discussed in Section 3.4). The upper WRA horizons in both sites contain shard counts that are an order of magnitude higher than the other WRA layers within these cores; therefore, they have been assumed to represent the primary deposition of the

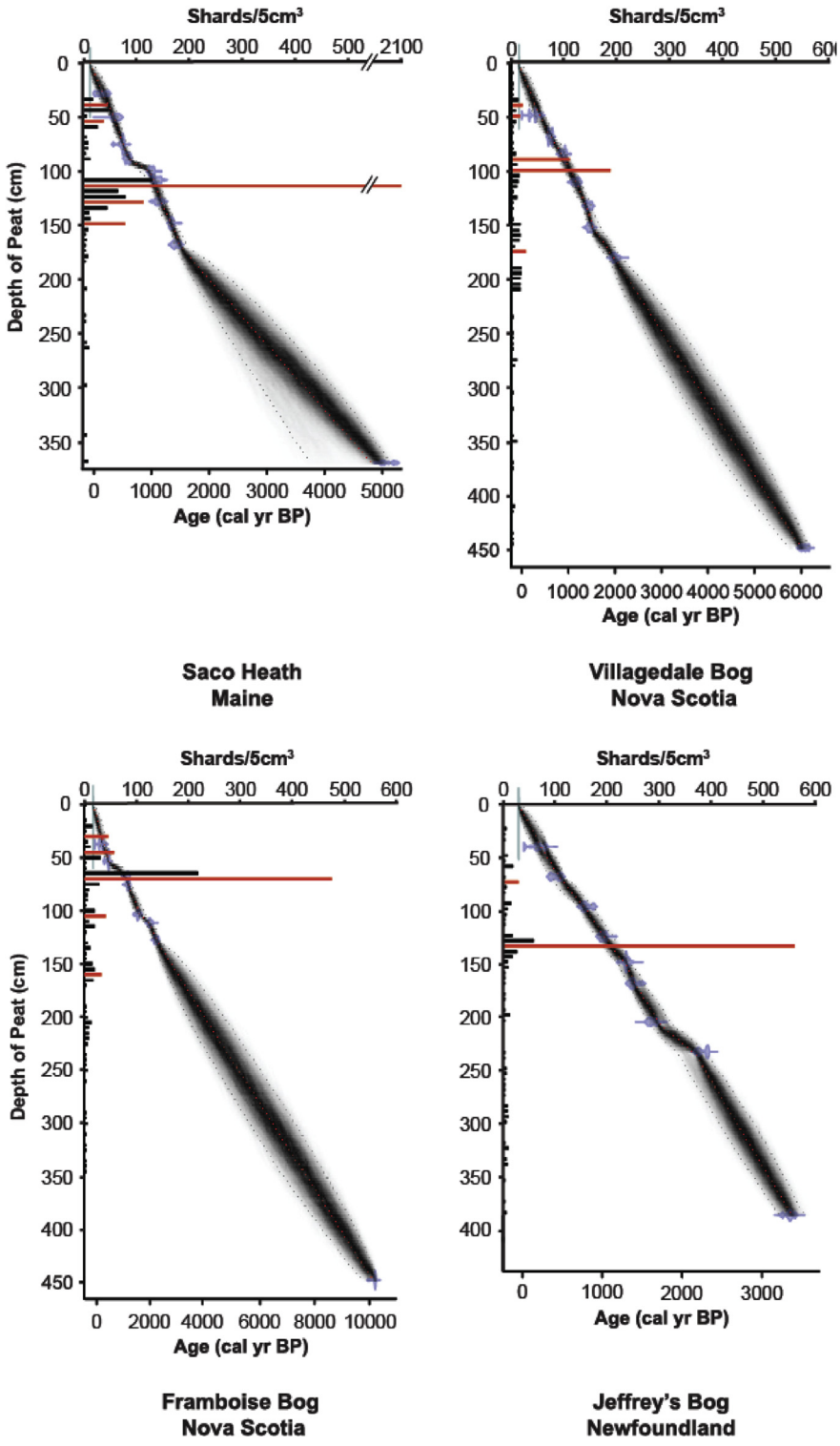

Fig. 2. Tephrostratigraphies from the four study sites. Shard concentrations are rhyolitic shards/5 cm^3 and layers extracted for EPMA analyses are highlighted in red. Higher resolution shard concentration data are provided in Appendix A, Supplementary Information. The radiocarbon age-depth models indicate results from Markov Chain Monte Carlo iterations completed in Bacon (Appendix D, Supplementary Information). The darker areas represent the most likely age ranges. (For interpretation of the references to colour in this figure legend, the reader is referred to the web version of this article.)

WRAe eruption. All core chronologies within this study (based on modelled ^{14}C measurements) provide age estimates that encompass the GICC05 date and further support the assumption that the upper WRA layers in SCH10 and FBB12 do represent the primary deposition of WRAe. The detection of this cryptotephra at all four sites builds on the previous identification of the WRAe in Newfoundland (Pyne-O'Donnell et al., 2012) and shows its prevalence across the eastern seaboard of North America. The largest WRAe horizon is located in Maine (SCH10-118), with an order of magnitude more shards (2120 shards/5 cm^3) than the closest study

Table 1
Means and standard deviations of single-grain glass compositions from cryptotephra layers. All data are normalised. n = number of analyses.

Sample		SiO_2	TiO_2	Al_2O_3	FeOt	MnO	MgO	CaO	Na_2O	K_2O	H_2O diff	n
SCH10-42	Mean	70.12	0.46	15.63	2.89	0.07	0.82	3.07	5.07	1.86	0.78	6
Pop. 1	StDev	1.74	0.05	1.21	0.23	0.01	0.16	0.40	0.32	0.14	2.16	
SCH10-42	Mean	75.89	0.27	13.19	1.44	0.04	0.18	1.22	4.20	3.57	3.04	3
Pop. 2	StDev	1.62	0.24	1.93	0.59	0.01	0.08	0.66	0.37	0.17	1.86	
SCH10-57	Mean	70.74	0.39	14.94	2.73	0.11	0.65	2.75	4.80	2.88	1.21	4
	StDev	0.41	0.01	0.18	0.14	0.02	0.02	0.16	0.29	0.07	1.65	
SCH10-118	Mean	74.06	0.19	14.22	1.54	0.05	0.40	1.93	4.35	3.27	3.51	26
	StDev	0.51	0.02	0.48	0.16	0.01	0.04	0.11	0.19	0.09	1.81	
SCH10-131	Mean	74.06	0.18	14.44	1.45	0.05	0.37	1.87	4.35	3.23	2.87	15
	StDev	0.84	0.03	0.56	0.20	0.01	0.06	0.17	0.21	0.12	1.87	
SCH10-150	Mean	73.79	0.20	14.70	1.54	0.05	0.39	1.89	4.29	3.15	2.56	13
	StDev	0.23	0.01	0.40	0.12	0.01	0.02	0.08	0.20	0.07	1.94	
VDB12-42	Mean	70.44	0.48	15.26	2.96	0.06	0.80	3.13	5.03	1.83	2.31	11
	StDev	0.58	0.04	0.24	0.34	0.01	0.19	0.18	0.29	0.16	1.31	
VDB12-53	Mean	75.67	0.38	12.72	2.26	0.06	0.33	2.60	3.85	2.12	0.50	2
	StDev	0.65	0.01	0.34	0.07	0.01	0.03	0.72	0.26	0.08	0.67	
VDB12-90	Mean	71.64	0.26	15.46	1.94	0.10	0.37	1.36	5.37	3.49	2.25	23
	StDev	0.50	0.02	0.37	0.12	0.01	0.04	0.11	0.22	0.11	1.39	
VDB12-100	Mean	74.38	0.17	14.26	1.42	0.04	0.35	1.81	4.27	3.30	3.05	15
	StDev	0.95	0.03	0.61	0.19	0.00	0.08	0.18	0.25	0.15	1.89	
VDB12-176	Mean	73.76	0.36	13.96	2.64	0.12	0.49	2.23	5.03	1.40	2.16	9
	StDev	0.63	0.03	0.62	0.34	0.01	0.08	0.16	0.22	0.07	2.15	
FBB12-31	Mean	72.52	0.37	14.62	2.37	0.05	0.61	2.47	4.81	2.17	2.72	12
	StDev	1.63	0.07	0.77	0.37	0.01	0.16	0.45	0.24	0.20	2.57	
FBB12-47	Mean	76.58	0.21	12.95	1.53	0.03	0.25	1.45	4.44	2.55	2.37	2
	StDev	0.23	0.01	0.07	0.07	0.00	0.02	0.14	0.22	0.15	0.28	
FBB12-70	Mean	74.90	0.17	13.76	1.47	0.04	0.34	1.84	4.22	3.24	4.14	23
	StDev	0.97	0.06	0.71	0.34	0.01	0.10	0.29	0.32	0.38	1.44	
FBB12-105	Mean	74.84	0.19	14.08	1.44	0.04	0.35	1.79	4.18	3.10	2.50	14
	StDev	0.79	0.03	0.55	0.20	0.01	0.06	0.24	0.37	0.30	2.25	
FBB12-162	Mean	76.72	0.34	11.86	2.21	0.06	0.44	2.40	3.64	2.34	3.10	5
	StDev	0.34	0.03	0.24	0.07	0.01	0.02	0.19	0.16	0.04	1.61	
JRB12-71	Mean	76.29	0.22	13.29	1.45	0.03	0.23	1.39	4.55	2.55	1.55	18
	StDev	0.79	0.02	0.66	0.11	0.01	0.04	0.23	0.27	0.15	1.66	
JRB12-131	Mean	74.32	0.19	14.25	1.49	0.05	0.36	1.87	4.20	3.28	2.56	27
	StDev	0.49	0.03	0.38	0.13	0.01	0.05	0.14	0.18	0.10	1.91	

Table 2
Means and standard deviations of single-grain glass compositions from reference material of potential correlatives, all data are normalised, n = number of analyses. Data sources: MSH-Wn and MSH-We: Pyne-O'Donnell et al. (2012) and Jensen et al. (2014b); MSH Layer T: Jensen et al. (2014b) and this study; Ceboruco P1 and Ksudach KS1: this study; Tarumai Ta-c2: Nanayama et al. (2003); WRAe: Pyne-O'Donnell et al. (2012) and Jensen et al. (2014a); WRAn: Jensen (2007).

Sample		SiO_2	TiO_2	Al_2O_3	FeOt	MnO	MgO	CaO	Na_2O	K_2O	Cl	H_2O diff	n
MSH-Wn	Mean	74.83	0.19	14.32	1.61	0.04	0.30	1.70	4.63	2.32	0.08	2.75	83
	StDev	0.42	0.03	0.44	0.10	0.03	0.03	0.08	0.25	0.11	0.03	2.45	
MSH-We	Mean	75.89	0.25	13.51	1.50	0.04	0.26	1.44	4.50	2.50	0.10	2.61	66
	StDev	0.50	0.04	0.27	0.08	0.03	0.03	0.12	0.19	0.09	0.03	1.94	
MSH	Mean	70.80	0.44	15.69	2.88	0.06	0.72	2.89	4.69	1.93	0.12	1.80	62
Layer T	StDev	1.52	0.08	0.73	0.43	0.03	0.17	0.54	0.31	0.21	0.04	1.78	
Ceboruco	Mean	71.44	0.28	15.94	1.96	0.09	0.34	1.34	5.13	3.39	0.102	1.89	25
P1	StDev	0.21	0.05	0.14	0.07	0.03	0.03	0.04	0.16	0.09	0.03	1.05	
Ksudach	Mean	73.32	0.40	13.97	2.67	0.16	0.45	2.22	5.22	1.35	0.17	2.54	28
KS1	StDev	1.14	0.09	0.75	0.53	0.06	0.14	0.31	0.53	0.10	0.02	1.38	
Tarumai	Mean	76.47	0.34	11.94	2.15	0.04	0.46	2.27	3.97	2.36	–	2.20	15
Ta-c2	StDev	0.82	0.04	0.22	0.29	0.02	0.14	0.26	0.08	0.12	–	1.04	
WRA east	Mean	73.89	0.21	14.49	1.52	0.05	0.36	1.83	4.13	3.19	0.34	2.73	107
(WRAe)	StDev	0.63	0.04	0.32	0.20	0.02	0.07	0.18	0.16	0.17	0.04	1.48	
WRA north	Mean	73.96	0.21	14.41	1.61	0.06	0.33	1.77	4.10	3.23	0.32	2.69	50
(WRAn)	StDev	1.16	0.07	0.53	0.25	0.03	0.08	0.30	0.18	0.15	0.05	1.54	

site Villagedale Bog, Nova Scotia. Whilst local conditions generate variable intra-peatland shard concentrations (Watson et al., 2015), the observed distribution of the WRAe within this study suggests that the southernmost limit of this ash has not yet been located. This may indicate that there is an opportunity to extend the tephra distribution map in North America and connect archives across greater distances.

3.2. Potential correlations

The following potential correlations are based on major-element geochemistry, age data, and glass morphology where reference material was available. Additional access to proximal reference materials and/or data, and trace-element geochemistry could help confirm these correlations.

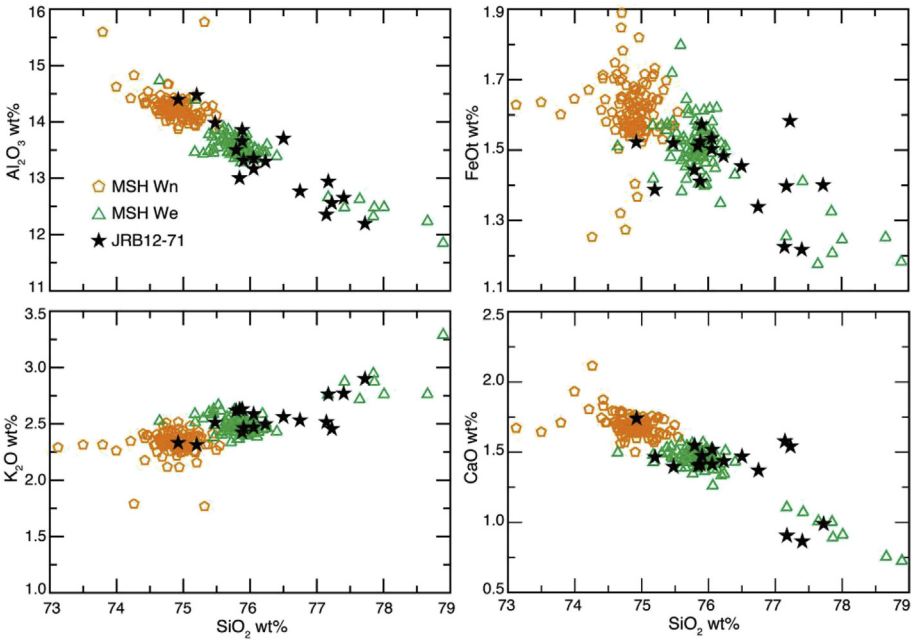

Fig. 3. Harker diagrams comparing the major element glass compositions of MSH-Wn, MSH-We and JRB12-71. JRB12-71's composition mirrors the geochemical trend seen in MSH-We.

3.2.1. FBB12-31 (AD 1565–1830)

Major and minor element geochemistry of FBB12-31 match well with data collected on both proximal and more distal reference samples of MSH layer T (Fig. 5). This tephra was deposited in AD 1799–1800 (Yamaguchi, 1983) and it is associated with the Mount St. Helens Goat Rocks eruptive period (Mullineaux, 1996). Layer T formed a narrow lobe limited to the northeast of the volcano and although thickness and grain-size rapidly decrease away from source, it has been reported as a visible unit up to 500 km from the source (Mullineaux, 1996). The glass morphology (pumiceous shards with the occasional bubble-walled shards) and the 2σ modelled age range of FBB12-31 confirm the similarity of this horizon to layer T. The correlation is also supported by the lack of other Mount St. Helens eruptions that fall into the required age range (e.g. MSH set X, ash bed Z or set W) with this specific composition (Mullineaux, 1996; Jensen et al., unpublished data).

3.2.2. FBB12-162 (3604–2643 cal yr BP)

This layer is characterised by pumiceous shards. Only seven analyses were successfully completed, of which two appear to be potentially unrelated to the main population. The remaining analyses characterise a high-SiO_2 rhyolite (~76–77 wt%) that has relatively low Al_2O_3, but high FeO_t and CaO for this SiO_2 concentration in comparison with available glass compositional data from Alaska, Cascades (Appendix F, Supplementary Information), Iceland (Tephrabase, Newton et al., 1997) and Kamchatka (Vera Ponomareva, pers. comm., 2014) in this age range. Comparisons with Japanese glass chemistries (Hughes et al., 2013; Nanayama et al., 2003) indicate that Hokkaido is a possible source region for this tephra (Fig. 6; Appendix C.3, Supplementary Information). Biplots of K_2O and TiO_2 concentrations have proved useful for distinguishing between Hokkaido regional volcanoes (Aoki and Machida, 2006; Furukawa et al., 1997; Tokui, 1989); however, comparisons between the FBB12-162 and proximal ash are limited both by the number of cryptotephra shards analysed from FBB12 and the lack of published individual proximal shard chemistries. FBB12-162 has greater geochemical similarities with the proximal ash from Tarumai than that from Komagatake. This potential correlation is supported by the age of the Tarumai tephra Ta-c2 (3000-2000 cal yr BP; Sato, 1971; Nanayama et al., 2003) that is comparable to the modelled age of FBB12-162. However, the lack of reference data precludes the firm correlation with Tarumai. The geochemical characteristics of two shards from VDB12-53 also show similarities with Japanese tephra (Table 1; Appendix C.3, Supplementary Information); however, the number of successfully typed shards and the exhaustion of core material prevent a firm correlation.

3.2.3. VDB12-176 (2055–1771 cal yr BP)

This horizon is characterised by pumiceous, sometimes blocky shards. The glass composition of this unknown tephra is strikingly similar to Ksudach 1 from the eastern volcanic front of the Kamchatka Peninsula (KS1; Fig. 7A–B). Ksudach is a large shield volcano with five overlapping calderas (Volynets et al., 1999). The eruption of KS1 in *ca.* 1800 cal yr BP was Kamchatka's second largest Holocene eruption (Braitseva et al., 1997), containing three proximal fall units of white or yellow pumice, density current deposits and a fall unit of grey pumice (Andrews et al., 2007; Braitseva et al., 1996). Initially, ash was deposited to the north but during the early phases of the eruption it travelled eastward until the final stages when it shifted westward (Melekestsev et al., 1996). Fall units can be identified over 1000 km from the source covering an area of 2–3 million km^2 (Braitseva et al., 1996). Glass morphology, composition and similar age estimates strongly support this correlation.

3.2.4. VDB12-90 (AD 889–1130)

The geochemistry in this horizon does not match any known eruptions of this age from Alaska, the Cascade Range (Appendix F, Supplementary Information), Kamchatka (Vera Ponomareva, pers. comm., 2014), Iceland (Tephrabase, Newton et al., 1997) or Japan (Appendix C.3, Supplementary Information). However, examination of published geochemical data available from Mexican sources showed that the chemistry closely resembled the main Plinian fall deposit (P1) of the Jala Pumice, which was deposited by the caldera-forming eruption of Volcán Ceboruco, AD 990–1020

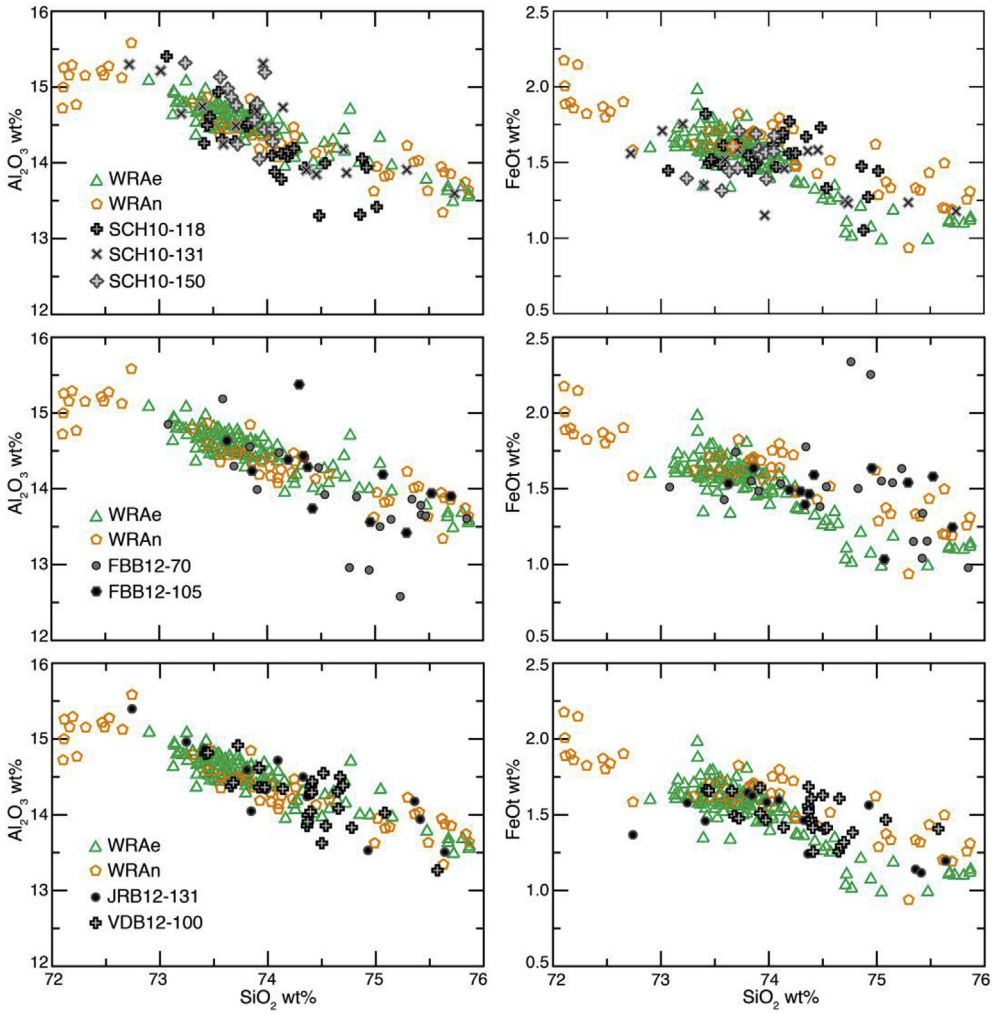

Fig. 4. Selected major element glass geochemical plots of proximal White River Ash (east and north lobe) and correlated cryptotephras. Most samples tend to cluster with the main WRAe geochemical population of ~73–74.5 SiO_2 wt%.

(Chertkoff and Gardner, 2004; Gardner and Tait, 2000; Sieron and Siebe, 2008). Volcán Ceboruco is located *ca.* 4400 km from the peatland in southeastern Nova Scotia, making the distance of ash transport *ca.* 800 km less than that between Mount Bona-Churchill (WRAe) and VDB12. Re-analysis of lapilli from the upper part of the P1 proximal deposit, collected at Locality 18 in Fig. 1 of Gardner and Tait (2000), confirm that VDB12-90 and P1 chemistry share striking similarities (Fig. 7C–F). The geochemical data are supported by the VDB12 core chronology. Therefore, it seems likely that VDB12-90 represents a distal deposit of the Jala Pumice from Volcán Ceboruco.

The potential for eastward dispersion of ash from Volcán Ceboruco was demonstrated using the UK Met Office's Numerical Atmospheric-dispersion Modelling Environment (NAME; Jones et al., 2007). To test the variability in ash transport directions, a large (up to 30 km in plume height) ten-day constant eruption of Volcán Ceboruco was assumed and a small random meteorological sample (current 10 days of meteorology) was used to track the particle dispersion through the modelled lower atmosphere. Whilst the AD 990–1020 eruption of Volcán Ceboruco may have been smaller than the modelled eruption and likely occurred during different meteorological conditions than those of today, the modelling results reveal the potential for the main ash plume to extend eastwards into Africa whilst a secondary plume splits from the main plume over the North Atlantic Ocean, extending northeastwards across Nova Scotia (Appendix G, Supplementary Information). Tephra transportation from Mexico to Nova Scotia may also occur when anticyclonic advection merges with a strongly meridonal polar jet stream, as modelled using weather and climate observations from NASA's MERRA dataset (NASA, 2012). Furthermore, there are precedents for Mexican tephras reaching the North Atlantic region, since ash from the *ca.* AD 1250–1400 (Palais et al., 1992) and AD 1982 (Zielinski et al., 1997) eruptions of El Chichón have been detected in the Summit region of Greenland.

3.3. Unidentified tephra horizon

3.3.1. VDB12-42 (AD 1517–1750) and SCH10-42 (AD 1572–1762)

The shard morphology of horizons VDB12-42 and SCH10-42 are dominated by pumiceous shards accompanied by occasional brown coloured shards. Although these rhyo-dacitic tephras (Fig. 8; Appendix E, Supplementary Information) fall within the compositional range of known Icelandic and Aleutian tephra and share similar glass morphological characteristics with them, they have not been correlated and have been provisionally termed here as the 'Villagedale tephra'. The Villagedale tephra and the WRAe are the only two tephras characterised within this study that have been detected in more than one study site.

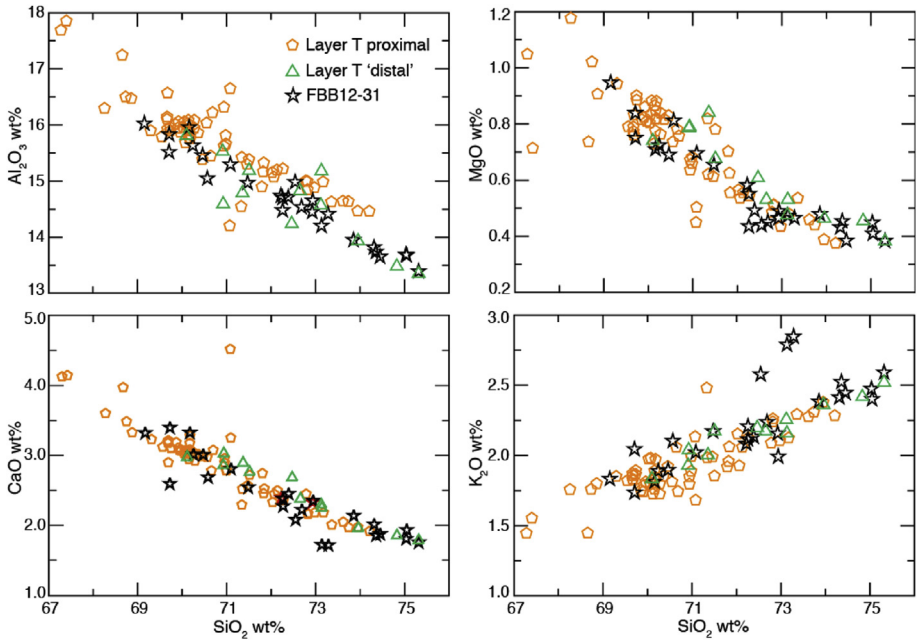

Fig. 5. Major and minor element glass compositions of proximal lapilli and distal ash from Mount St Helens layer T and the potential correlative FBB12-31. The proximal data comprise multiple samples that represent the entire event. The distal sample is a visible ash deposit several hundred kilometres distant in NE Washington State.

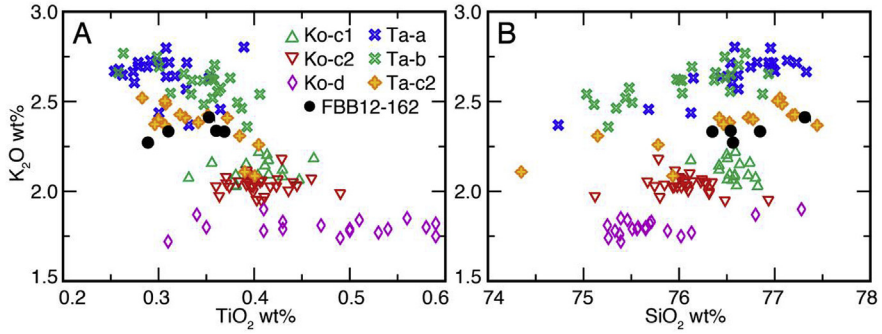

Fig. 6. Geochemical plots of FBB12-162 in comparison with tephra from the Tarumai (Ta) and Komagatake (Ko) volcanoes of Hokkaido, Japan. Single grain analyses of the historic eruptions Ko-c1,c2 and Ta-a,b,c2 are from Nanayama et al. (2003) and Ko-d data are from Hughes et al. (2013). Traditionally, Ko and Ta tephra are separated from each other on a K_2O and TiO_2 biplot, FBB12-162 plots in the field defined by Ta. B – Plotting K_2O vs. SiO_2 also shows more clearly that FBB12-162 plots more closely with Ta-c, which in terms of age is the most likely correlative. Dates of eruptions: Ta-a: AD 1739 (Yamada, 1958); Ta-b: AD 1667 (Yamada, 1958); Ta-c2: 2000–3000 cal yr BP (Sato, 1971); Ko-c1: AD 1856 (Yamada, 1958); Ko-c2: AD 1694 (Furukawa et al., 1997; Yamada, 1958).

3.4. Multiple within-core White River Ash horizons

One caveat related to the use of isochrons is demonstrated in the stratigraphy of SCH10 and FBB12, which register multiple layers of elevated tephra concentrations that geochemically correlate with the WRA (Fig. 4; Appendix C.2, Supplementary Information). The overlapping geochemistry, representing a single volcanic centre, complicates both the assignment of an age within stratigraphies and the degree of precision when correlating with other records. Therefore, under these conditions the isochron may represent a 'passage in time' rather than a 'moment in time' (*sensu* Dugmore et al., 2004). SCH10 contains three horizons that are distinct at both 5 cm and 1 cm resolutions and FBB12 contains two horizons that are separated by 35 cm of peat accumulation with low or zero background shard counts (Fig. 2; Appendix A, Supplementary Information). Since the upper WRA tephra horizons of SCH10-118 and FBB12-70 are an order of magnitude larger than the other within-core WRA horizons, they have been assumed to represent the main WRAe eruption.

Two main factors may have contributed to the multiple WRA horizons: firstly, there may be several eruption events/stages from the same volcanic centre (Preece et al., 2014) and secondly, post-depositional movement of the shards may have occurred (e.g. Payne and Gehrels, 2010; Swindles et al., 2013; Watson et al., 2015). Although atmospheric conditions also influence site-specific delivery of ash layers (since circulation and localised precipitation patterns can result in intermittent shard deposition (Davies et al., 2010; Dugmore and Newton, 1997; Payne et al., 2013; Pyne-O'Donnell, 2011)), delayed atmospheric transport of shards cannot explain this multiple peak feature. Peat accumulation rates in oceanic settings are usually around 10 yr/cm, whereas the maximum atmospheric retention time of ash clouds is in the order of 1–2 years (Cole-Dai et al., 2000, 2009; Fiacco et al., 1994; Robock, 2002; Zielinski et al., 1994).

Multiple eruptions are a possible explanation for the observed SCH10 and FBB12 pattern since two eruptions from Mount

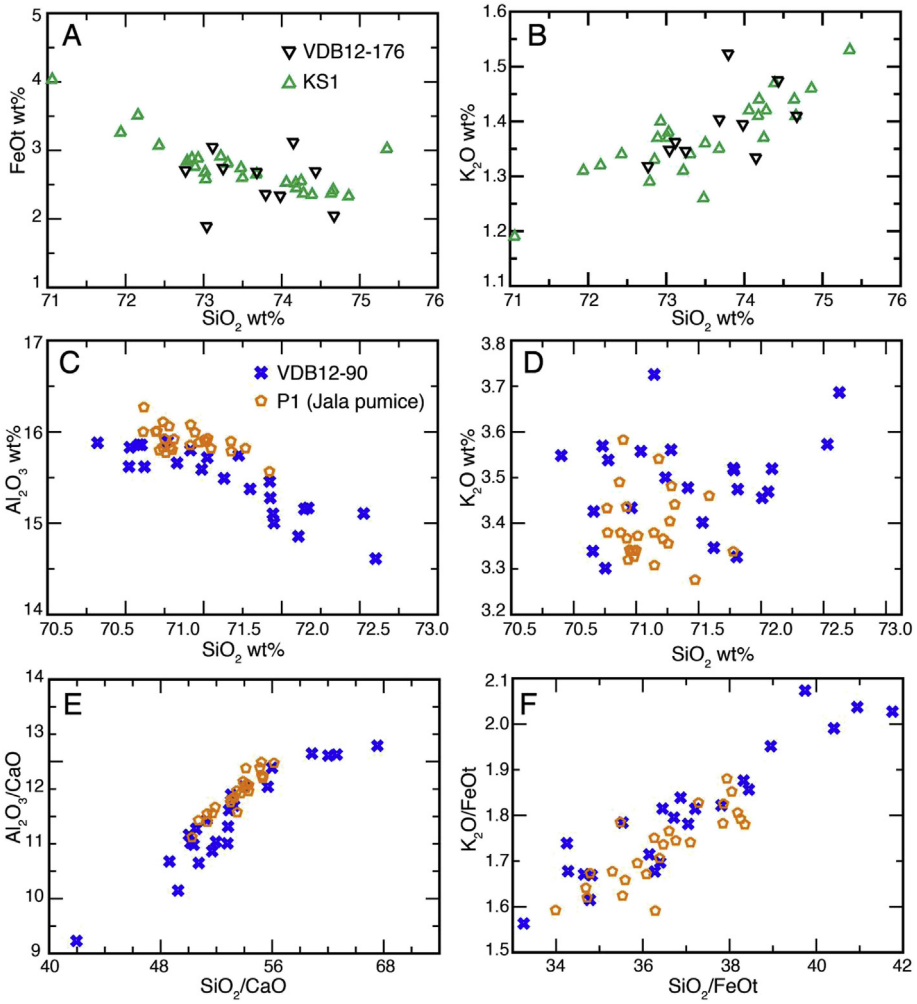

Fig. 7. Major-element glass compositions of: A–B – Ksudach 1 from visible ash deposits collected in Kamchatka plotted with VDB12-176, all oxides are virtually identical, as illustrated in these two Harker diagrams; C, D – Glass analyses from crushed lapilli of P1 from Volcán Ceboruco plotted with VDB12-90. All oxides plot together within analytical error, although some oxides, Al_2O_3 in particular, have a slight, but visible, offset. The difference seen between the two samples is likely the result of calibration differences, Lipari standard data bracketing VDB12-90 shows lower than average Al_2O_3 wt% values, while standard data bracketing P1 analyses were higher than average. E, F – If the ratios between the elements in each sample remain similar regardless of the calibration error, and if the two samples are indeed the same, plotting the data as ratios may help eliminate some of the offset caused by that error, which appears to be the case here.

Churchill have been reported around the time period of interest: the prominent eastern lobe (AD 847 ± 1; Jensen et al., 2014a) and the smaller northern lobe (*ca.* 1560–1680 cal yr BP; Froese and Jensen, 2005). This hypothesis cannot be fully tested here since the dataset is limited by the low initial shard concentrations and the exhaustion of sample material, thus preventing further analysis of any subtle geochemical differences between the two Mount Bona-Churchill layers. The ^{14}C-modelled age of FBB12-105 is *ca.* 1673 cal yr BP and there is distinct stratigraphic separation of the two FBB12 WRA layers with low tephra concentrations in-between (Fig. 2; Appendix A, Supplementary Information); therefore, a multiple-eruption explanation is possible. However, the ^{14}C-modelled age of tephra deposition at SCH10-150 is *ca.* 1363 cal yr BP; therefore, it is unlikely that this WRA layer originated from the northern lobe of the WRA.

The age discrepancies between SCH10-150 and the known WRA eruptions indicate that the multiple WRA layers detected within SCH10 may be explained either by the presence of an additional uncharacterised WRA eruption or by post-depositional movement of tephra shards. The potential for vertical tephra movement within peat has been demonstrated in field and laboratory experiments (Payne et al., 2005; Payne and Gehrels, 2010), as well as a study of naturally deposited tephra in disturbed peatlands (Swindles et al., 2013). Such post-depositional movement is influenced by a variety of local factors associated with physical peat properties, peat hydrological conditions, meteorological conditions and disturbance events, as summarised by Watson et al. (2015).

Water table fluctuations may have contributed to downward vertical tephra transport in SCH10; however, the distance of such transport that is required to explain the observed tephra horizon patterns have not been confirmed by field experiments (Payne et al., 2005). Shard movement may also have been encouraged by vegetation dynamics at the peat surface: root channels have been attributed to providing pathways for shards to be deposited downwards in lake sediments (e.g. Davies et al., 2005, 2007) and *Sphagnum*-dominant peat can act as efficient tephra traps (Watson et al., 2015). The macrofossil composition of JRB12 is consistently dominated by *Sphagnum* (*ca.* 75–85%) and similar *Sphagnum* abundance values are evident throughout VDB12 (except between 68 and 84 cm which registers an increase in Ericaceae and monocotyledon plant remains; Mackay et al., 2013). These moss-dominated conditions may, therefore, limit the translocation of

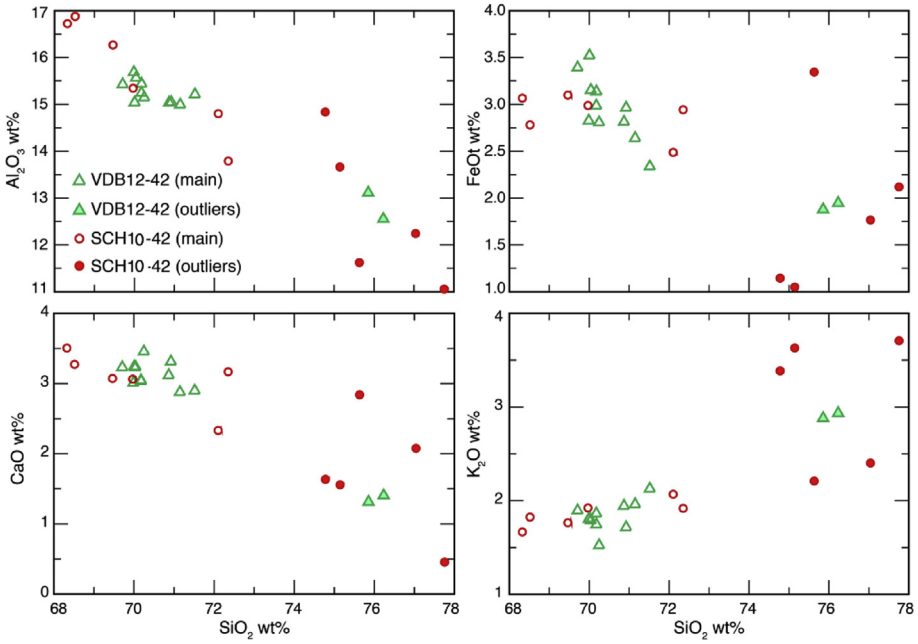

Fig. 8. Major-element glass compositions of VDB12-42 and SCH10-42. Comparable ages and glass compositions between the lower SiO_2 wt% population of the tephras suggest a potential correlation. The higher SiO_2 wt% values (>74 wt%) are quite scattered and probably largely represent shards that may be from different eruptions.

tephra shards as is indicated by the lack of multiple ash layers in the tephrostratigraphies of these sites. In contrast, SCH10 registers fluctuating phases of Ericaceae dominance (*ca.* 50%), one period of which occurs after the WRA deposition between 88 and 108 cm (Mackay et al., 2013). The increase of such shrub species with penetrating roots enhances the possibility of post-depositional tephra movement. The considerable concentrations of tephra shards in the upper two WRA-type horizons in SCH10 may exacerbate any post-depositional movement of shards and may also explain why the apparent movement is greater here than at the other study sites.

4. Conclusions

This study has expanded the known geographical range of cryptotephra deposition in eastern North America and has revealed more ash layers, from more varied source regions, than previously identified. This not only increases the potential chronological control provided by the tephras, but also increases the geographical areas with which palaeoenvironmental records can be synchronised. The potential of linking palaeoenvironmental records across the tropics and the mid-to high latitudes presents exciting opportunities to explore changes in interregional atmospheric and oceanographic circulation patterns.

The White River Ash (eastern lobe) from Mount Bona Churchill is confirmed as a dominant isochron and the scope for its spatial extension across the eastern seaboard of North American has been presented. The recent correlation of the WRAe to the "AD860B" ash found in Greenland and northern Europe (Jensen et al., 2014a) and the extended eastern North America distribution of the WRAe presented in this study highlights the importance of this tephra as an intercontinental temporal link between environmental archives. Future palaeoenvironmental studies may therefore utilise the extended WRAe distribution to investigate reconstructed climate change associated with the Medieval Climate Anomaly (MCA; AD 900–1350) in eastern North America. Comparisons of such reconstructions with records from Greenland and western Europe may identify potential MCA climatic drivers, such as changes in the strength of the Gulf Stream and Labrador Current, enhancing our understanding of the climate system during the MCA as a partial-analogue for future climate warming.

The deposition of the WRAe in Newfoundland also coincides with a time of regional archaeological change: the L'Anse aux Meadows area was intermittently occupied by the Middle Dorset cultures before the settlement of the Recent Indians (*ca.* AD 670–990; Davis et al., 1988; Wallace, 2003). Following the departure of the Recent Indians, a temporary Norse settlement was constructed *ca.* AD 990–1050 (Wallace, 1991), documenting the first European presence in North America. Whilst the current study sites do not extend into northern Newfoundland, the potential for a more northerly WRAe distribution should be recognised. Future research may therefore focus on identifying the WRAe in archaeological and environmental archives from Newfoundland's Great Northern Peninsula with the aim of refining regional settlement chronologies and establishing the extent to which climatic change was responsible for regional population changes.

The White River Ash eastern lobe is the only correlated tephra detected in multiple sites within this study and can, therefore, act as an isochronous marker. The single-site distribution of the other correlated tephras could indicate that their deposition was confined to narrow geographical areas in eastern North America. Alternatively, a combination of regional and local factors may be generating patchy distribution of tephra deposition across sites (Watson et al., 2015). Targeting specific peat depths of ages contemporary with known eruptions could identify whether the tephras are absent from the sites or whether they are present in low concentrations. However, the low shard concentrations typical of the sites within this study would likely limit the effectiveness of this approach. For example, FBB12-47 contains 15 shards/cm^3 and has a modelled 2σ age range of AD 1374–1677, which encompasses the dates of Mount St Helens set W eruptions (Yamaguchi, 1985; Fiacco et al., 1993; Mullineaux, 1996). Only two shards were successfully extracted and analysed from this layer; therefore, despite chronological and geochemical similarities, there is insufficient

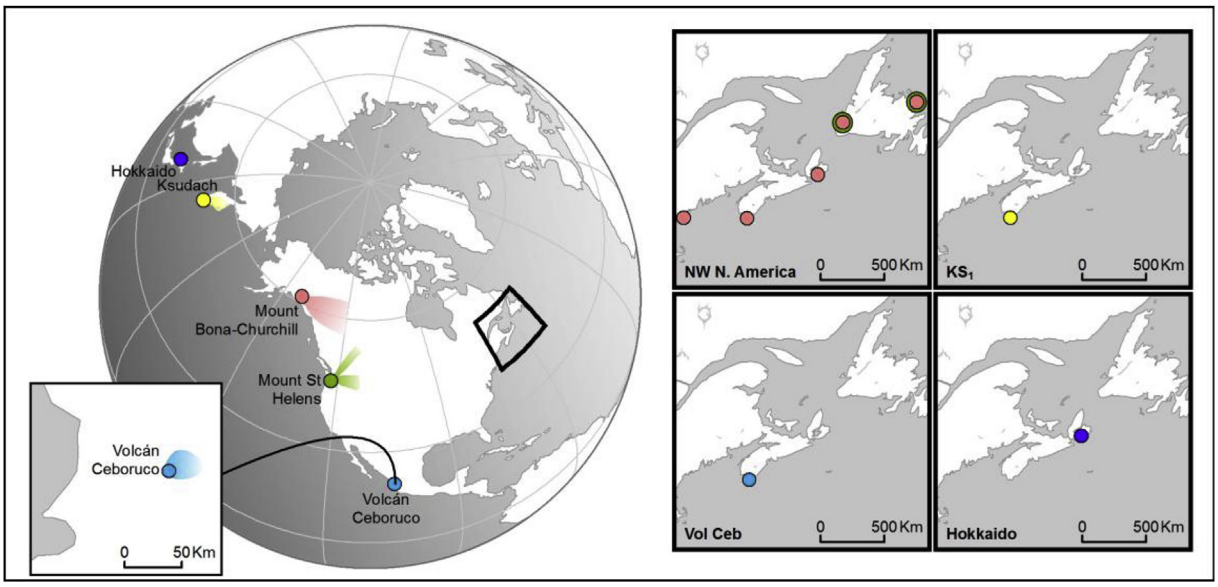

Fig. 9. Eastern North American cryptotephra lattice: sites from this study and Nordan's Pond Bog (Pyne-O'Donnell et al., 2012).

data to conclusively conclude that the FBB12-47 cryptotephra horizon originated from Mount St Helens W. Future studies may consider sampling multiple sites within multiple regions to distinguish between tephras that have been deposited in narrow geographical envelopes and those which are characterised by intermittent deposition.

The incorporation of the correlated tephra data into the age-depth models substantially improves the precision of the modelled core chronologies. For example, when the WRAe GICC05 age and ^{14}C measurements are used to construct the age-depth models, the average chronological error for each 1 cm interval in the 200-year period surrounding the depth of WRAe deposition is half of the error generated when only ^{14}C measurements are used (Appendix H). A more dramatic example of chronological refinement through the incorporation of tephra data is evident in FBB12 and the age control provided by the near-surface MSH layer-T tephra. The average age-depth model error in the 200-year period surrounding the depth of layer-T deposition is reduced from 248 years to 71 years (Appendix H). These examples highlight the utility of conducting tephra analysis in studies comparing environmental change, even if the tephras cannot be used as fixed tie-points between sites.

Mexican and East Asian tephras reaching the eastern seaboard of North America provide an exciting prospect for expanding the region's tephra framework. Data from additional sites, the improved availability of proximal geochemical reference datasets and the incorporation of trace element data will facilitate the characterisation of tephra distributions from these source regions. Two further cryptotephras have been located in eastern North America: Mount St Helens layer T and the newly identified Villagedale tephra; however, more data are again required to confirm and constrain these layers. This lack of comparative data will likely be the limiting factor in future cryptotephra studies; therefore, investigating proximal ashes and enhancing the content and availability of comparative databases is essential for extending tephra frameworks (*sensu* Kuehn et al., 2013).

This study highlights the caution required when interpreting multiple tephra horizons from the same eruption centre for use as isochrons. With appropriate caution, the prevalence of cryptotephra layers found in eastern North America facilitates the construction of a regional tephra lattice (Fig. 9), which will expand as more records are developed and the region's tephrochronological wealth is uncovered.

Author contributions

Helen Mackay, Paul Hughes and Pete Langdon conceived and designed the study. Helen Mackay performed the research, analysed the cryptotephra with guidance from Sean Pyne-O'Donnell and wrote the paper with editorial input from the co-authors. North American and Mexican proximal tephra analyses were performed by Britta Jensen on reference material provided by Duane Froese and James Gardner (respectively). Kamchatkan analyses were performed by Gill Plunkett and Sarah Coulter. Data analysis was completed by Helen Mackay and Britta Jensen.

Acknowledgements

This research was funded by a Natural Environment Research Council (NERC) Tephra Analytical Unit grant (TAU 79/1012); the NERC funded PRECIP project (grant numbers NE/G019851/1, NE/G02006X/1; NE/G020272/1; NE/G019673/1); the NERC funded MILLIPEAT project (grant number NE/1012915/1); a Quaternary Research Association New Research Workers award granted to H. Mackay and a Natural Sciences and Engineering Research Council (NSERC) of Canada Discovery grant held by D.G. Froese. This work was supported by the NERC Radiocarbon Facility NRCF010001 (allocation numbers 1744.1013 and 1789.0414). Kamchatkan samples were collected as part of a project led by Prof. Keith Bennett and funded by the Swedish Research Council. We would like to thank Chris Hayward at the Tephrochronology Analytical Unit (TAU), University of Edinburgh for his help and advice during microprobe work and to Mike Hall (University of Edinburgh) for the completion of tephra stubs. Siwan Davies, Peter Abbott and Anna Bourne (Swansea University) and Alison MacLeod (Royal Holloway University of London) also provided much appreciated guidance during sample preparation. Thanks are due to Paul Carrara for providing the distal layer T sample, and Steve Kuehn for collecting the St. Helens proximal samples. We are grateful to Vera Ponomareva (Institute of Volcanology and Seismology, Russian Academy of Sciences) for comparing some data with Kamchatkan sources, to Victoria Smith (University of Oxford) for comparing data with

Mexican and Japanese sources and to Ryuta Furukawa for providing access to the point-by-point Japanese tephra data from Nanayama et al. (2003). Thanks to Tim Daley (Plymouth University) and Dan Charman (University of Exeter) for collecting the SCH10 core and to Gunnar Mallon (University of Sheffield) for fieldwork assistance. We are grateful to Mark Dover at the University of Southampton for assistance with Figs. 1, 2 and 9. We also thank Dr Graham Swindles, Dr. Brent Alloway, Dr. John Westgate and the anonymous reviewer for their helpful comments on the manuscript.

Appendix A. Supplementary data

Supplementary data related to this article can be found at http://dx.doi.org/10.1016/j.quascirev.2015.11.011.

References

Alloway, B.V., Lowe, D.J., Larsen, G., Shane, P.A.R., Westgate, J.A., 2013. Tephrochronology. In: Elias, S.A. (Ed.), The Encyclopedia of Quaternary Sciences, second ed., vol. 4. Elsevier, Amsterdam, pp. 277–304.

Andrews, B.J., Gardner, J.E., Tait, S., Ponomareva, V., Melekestsev, I.V., 2007. Dynamics of the 1800 14C yr BP caldera-forming eruption of Ksudach volcano, Kamchatka, Russia. In: Eichelberger, J., Gordeev, E., Kasahara, M., Izbekov, P., Lees, J. (Eds.), Volcanism and Subduction: the Kamchatka Region. Geophysical Monograph Series, vol. 172. American Geophysical Union, Washington DC, pp. 325–342.

Aoki, K., Machida, H., 2006. Major element composition of volcanic glass shards of the late Quaternary widespread tephra in Japan — distinction of tephras using K_2O–TiO_2 diagrams. Bull. Geol. Surv. Jpn. 57, 239–258 (in Japanese with English captions).

Blaauw, M., Christen, J.A., 2011. Flexible paleoclimate age-depth models using an autoregressive gamma process. Bayesian Anal. 6, 457–474.

Blockley, S.P.E., Pyne-O'Donnell, S.D.F., Lowe, J.J., Matthews, I.P., Stone, A., Pollard, A.M., Turney, C.S.M., Molyneux, E.G., 2005. A new and less destructive laboratory procedure for the physical separation of distal glass tephra shards from sediments. Quat. Sci. Rev. 24, 1952–1960.

Borchardt, G.A., Aruscavage, P.J., Millard, H.T., 1972. Correlation of the Bishop Ash, a Pleistocene marker bed using instrumental neutron activation analysis. J. Sediment. Petrol. 42, 301–306.

Braitseva, O.A., Melekestsev, I.V., Ponomareva, V.V., Kirianov, V.Yu, 1996. The caldera-forming eruption of Ksudach volcano about cal. AD 240, the greatest explosive event of our era in Kamchatka. J. Volcanol. Geotherm. Res. 70, 49–66.

Braitseva, O.A., Ponomareva, V.V., Sulerzhitsky, L.D., Melekestsev, I.V., Bailey, J., 1997. Holocene key-marker tephra layers in Kamchatka, Russia. Quat. Res. 47, 125–139.

Chertkoff, D.G., Gardner, J.E., 2004. Nature and timing of magma interactions before, during, and after the caldera-forming eruption of Volcán Ceboruco. Mex. Contribu. Mineral. Petrol. 146, 715–735.

Cole-Dai, J., Mosley-Thompson, E., Wight, S.P., Thompson, L.G., 2000. A 4100-year record of explosive volcanism from an East Antarctica ice core. J. Geophys. Res. 105 (D19), 24431–24441.

Cole-Dai, J., Ferris, D., Lanciki, A., Savarino, J., Baroni, M., Thiemens, M.H., 2009. Cold decade (AD 1810–1819) caused by Tambora (1815) and another (1809) stratospheric volcanic eruption. Geophys. Res. Lett. 36, L22703.

Coulter, S.E., Pilcher, J.R., Plunkett, G., Baillie, M., Hall, V.A., Steffensen, J.P., Vinther, B.M., Clausen, H.B., Johnsen, S.J., 2012. Holocene tephras highlight complexity of volcanic signals in Greenland ice cores. J. Geophys. Res. 117, D21303.

Davies, S.M., Hoek, W.Z., Bohncke, S.J.P., Lowe, J.J., Pyne O'Donnell, S., Turney, C.S.M., 2005. Detection of Lateglacial distal tephra layers in the Netherlands. Boreas 34, 123–135.

Davies, S.M., Elmquist, M., Bergman, J., Wohlfarth, B., Hammarlund, D., 2007. Cryptotephra sedimentation processes within two lacustrine sequences from west central Sweden. Holocene 17, 319–330.

Davies, S.M., Larsen, G., Wastegård, S., Turney, C.S.M., Hall, V.A., Coyle, L., Thordarson, T., 2010. Widespread dispersal of Icelandic tephra: how does the Eyjafjöll eruption of 2010 compare to past Icelandic events? J. Quat. Sci. 25, 605–611.

Davis, A.M., McAndrews, J.H., Wallace, B.L., 1988. Paleoenvironment and the archaeological record at the L'Anse aux Meadows Site, Newfoundland. Geoarchaeol. Int. J. 3, 53–64.

Dugmore, A.J., Newton, A.J., 1992. Thin tephra layers in peat revealed by X-radiography. J. Archaeol. Sci. 19, 163–170.

Dugmore, A.J., Newton, A.J., 1997. Holocene Tephra Layers in the Faroe Islands. Frodskaparrit Faroese J. Nat. Med. Sci. 4, 141–154.

Dugmore, A.J., Larsen, G., Newton, A.J., Sugden, D.E., 1992. Geochemical stability of fine-grained silicic Holocene tephras in Iceland and Scotland. J. Quat. Sci. 7, 173–183.

Dugmore, A.I., Newton, A.I., Edwards, K.I., Larsen, G., Blackford, J.J., Cook, G.T., 1996. Long-distance marker horizons from small-scale eruptions: British tephra deposits from the AD 1510 eruption of Hekla, Iceland. J. Quat. Sci. 11, 511–516.

Dugmore, A.J., Larsen, G., Newton, A.J., 2004. Tephrochronology and its application to late Quaternary environmental reconstruction, with special reference to the North Atlantic islands. In: Buck, C.E., Millard, A.R. (Eds.), Tools for Constructing Chronologies: Crossing Disciplinary Boundaries. Lecture Notes in Statistics, vol. 177. Springer, London, pp. 173–188.

Fiacco Jr., R.J., Palais, J.M., Germani, M.S., Zielinski, G.A., Mayewski, P.A., 1993. Characteristics and possible source of a 1479 A.D. Volcanic ash layer in a Greenland Ice Core. Quat. Res. 39, 267–273.

Fiacco Jr., R.J., Thordarson, T., Germani, M.S., Self, S., Palais, J.M., Whitlow, S., Grootes, P.M., 1994. Atmospheric aerosol loading and transport due to the 1783–1784 Laki eruption in Iceland, interpreted from ash particles and acidity in the GISP2 ice core. Quat. Res. 42, 231–240.

Froese, D.G., Jensen, B.J., 2005. Stop 2: White River Ash-eastern lobe. In: Froese, D.G., Westgate, J.A., Alloway, B.V. (Eds.), Field Trip Guide for the International Field Conference and Workshop on Tephrochronology and Volcanism, Dawson City, Yukon Territory, Canada. Institute of Geological and Nuclear Sciences, New Zealand, pp. 53–56. Science Report 2005/26.

Froggatt, P.C., 1983. Toward a comprehensive Upper Quaternary tephra and ignimbrite stratigraphy in New Zealand using electron microprobe analysis of glass shards. Quat. Res. 19, 188–200.

Furukawa, R., Yoshimoto, M., Yamagata, K., 1997. Did Hokkaido Komagatake Volcano Erupt in 1694? Reappraisal of the Eruptive Ages of 17th–18th Centuries in Hokkaido. Kazan 42, pp. 269–279.

Gardner, J.E., Tait, S., 2000. The caldera-forming eruption of Volcan Ceboruco, Mexico. Bull. Volcanol. 62, 20–33.

Goring, S., Williams, J.W., Blois, J.L., Jackson, S.T., Paciorek, C.J., Booth, R.K., Marlon, J.R., Blaauw, M., Christen, J.A., 2012. Deposition times in the eastern United States during the Holocene: establishing valid priors for Bayesian age models. Quat. Sci. Rev. 48, 54–60.

Hall, V.A., Pilcher, J.R., McVicker, S.J., 1993. Tephra-linked studies and environmental archaeology, with special reference to Ireland. Circaea J. Assoc. Environ. Archaeol. 11, 17–22.

Hayward, C., 2012. High spatial resolution electron probe microanalysis of tephra and melt inclusions without beam-induced chemical modification. Holocene 22, 119–125.

Hughes, P.D.M., Mallon, G., Brown, A., Essex, H.J., Stanford, J.D., Hotes, S., 2013. The impact of high tephra loading on late-Holocene carbon accumulation and vegetation succession in peatland communities. Quat. Sci. Rev. 67, 160–175.

Jensen, B.J.L., 2007. Tephrochronology of Middle to Late Pleistocene Loess in East-central Alaska. University of Alberta, p. 120 (MSc thesis).

Jensen, B.J.L., Pyne-O'Donnell, S., Plunkett, G., Froese, D.G., Hughes, P.D.M., Sigl, M., McConnell, J.R., Amesbury, M.J., Blackwell, P.G., van den Bogaard, C., Buck, C.E., Charman, D.J., Clague, J.J., Hall, V.A., Koch, J., Mackay, H., Mallon, G., McColl, L., Pilcher, J.R., 2014a. Transatlantic distribution of the Alaskan White River Ash. Geology 42, 875–878.

Jensen, B.J.L., Kuehn, S.K., Froese, D.G., 2014b. Geochemical Characterization of the Mount St. Helens "Spirit Lake" Stage. Tephra 2014-Maximizing the Potential of Tephra for Multidisciplinary Science, August 2014. Portland, OR.

Jones, A.R., Thomson, D.J., Hort, M., Devenish, B., 2007. The U.K. Met Office's next-generation atmospheric dispersion model, NAME III. In: Borrego, C., Norman, A.-L. (Eds.), Air Pollution Modeling and its Application XVII (Proceedings of the 27th NATO/CCMS International Technical Meeting on Air Pollution Modelling and its Application. Springer, pp. 580–589.

Kuehn, S.C., Foit, F.F., 2006. Correlation of widespread Holocene and Pleistocene tephra layers from Newberry Volcano, Oregon, using glass compositions and numerical methods. Quat. Int. 148, 113–137.

Kuehn, S.C., Froese, D.G., Shane, P.A.R., 2011. The INTAV intercomparison of electron-beam microanalysis of glass by tephrochronology laboratories, results and recommendations. Quat. Int. 246, 19–47.

Kuehn, S.C., Bursik, M.I., Pouget, S., 2013. Improved integration and discoverability of Tephra Data for multidisciplinary applications. In: Abstract V13A-2591 Presented at 2013 Fall Meeting, AGU, San Francisco (9–13 Dec 2013). http://abstractsearch.agu.org/meetings/2013/FM/sections/V/sessions/V13A/abstracts/V13A-2591.html (last accessed 19 Sept 2014).

Lane, C.S., Chorn, B.T., Johnson, T.C., 2013a. Ash from the Toba supereruption in Lake Malawi shows no volcanic winter in East Africa at 75 ka. PNAS 110, 8025–8029.

Lane, C.S., Brauer, A., Blockley, S.P.E., Dulski, P., 2013b. Volcanic ash reveals time-transgressive abrupt climate change during the Younger Dryas. Geology 41 (12), 1251–1254.

Lowe, D.J., 2011. Tephrochronology and its application: a review. Quat. Geochronol. 6, 107–153.

Lowe, D.J., Hunt, J.B., 2001. A summary of terminology used in tephra-related studies. Doss. l'Archaéo-Logis 1, 17–22.

Lowe, J., et al., 2012. Volcanic ash layers illuminate the resilience of Neanderthals and early modern humans to natural hazards. Proc. Natl. Acad. Sci. 109, 13532–13537.

Mackay, H., Hughes, P.D.M., Langdon, P.G., 2013. Constraining Peatland environmental change: exploiting the emerging Eastern North American Cryptotephrostratigraphic Record. In: Abstract PP13C-1897 Presented at 2013 Fall Meeting, AGU, San Francisco (9–13 Dec 2013). http://adsabs.harvard.edu/abs/2013AGUFMPP13C1897M (last accessed 28 Sept 2014).

Melekestsev, I.V., Braitseva, O.A., Ponomareva, V.V., Sulerzhitsky, L.D., 1996. Holocene catastrophic caldera-forming eruptions of Ksudach volcano. Kamchatka Volcanol. Seismol. 17, 395–421.

Mullineaux, D.R., 1996. Pre-1980 Tephra-fall Deposits Erupted from Mount St. Helens. U.S. Geological Survey, Washington, p. 99. Professional Paper 1563.
Nanayama, F., Satake, K., Furukawa, R., Shimokawa, K., Atwater, B.F., Shigeno, K., Yamaki, S., 2003. Unusually large earthquakes inferred from tsunami deposits along the Kuril trench. Nature 424, 660–663.
Newton, A.J., Gittings, B., Stuart, N., 1997. Designing a Scientific Database Query Server Using the World Wide Web: the Example of Tephrabase. Innovations in GIS 4. Taylor and Francis, London, pp. 251–266.
Palais, J.M., Germani, M.S., Zielinski, G.A., 1992. Inter-hemispheric transport of volcanic ash from a 1259 AD volcanic eruption to the Greenland and Antarctic Icesheets. Geophys. Res. Lett. 19, 801–804.
Payne, R.J., Gehrels, M.J., 2010. The formation of tephra layers in peatlands: an experimental approach. Catena 81, 12–23.
Payne, R.J., Kilfeather, A.A., van der Meer, J.J.M., Blackford, J.J., 2005. Experiments on the taphonomy of tephra in peat. Suoseura 64, 147–156.
Payne, R., Blackford, J., van der Plicht, J., 2008. Using cryptotephras to extend regional tephrochronologies: an example for southeast Alaska and implications for hazard assessment. Quat. Res. 69, 42–55.
Payne, R.J., Edwards, K.J., Blackford, J.J., 2013. Volcanic impacts on the Holocene vegetation history of Britain and Ireland? A review and meta-analysis of the pollen evidence. Veg. Hist. Archaeobotany 22, 153–164.
Pilcher, J.R., Hall, V.A., 1992. Towards a tephrochronology for the Holocene of the north of Ireland. Holocene 2, 255–259.
Plunkett, G., Swindles, G.T., 2008. Determining the Sun's influence on Late Glacial and Holocene climates: a focus on climate response to centennial-scale solar forcing at 2800 cal. BP. Quat. Sci. Rev. 2, 175–184.
Preece, S.J., McGimsey, R.G., Westgate, J.A., Pearec, N.J.G., Hart, W.K., Perkins, W.T., 2014. Chemical Complexity and Source of the White River Ash, Alaska and Yukon.
Pyne-O'Donnell, S.D.F., 2011. The taphonomy of Last Glacial-Interglacial Transition (LGIT) distal volcanic ash in small Scottish lakes. Boreas 40, 131–145.
Pyne-O'Donnell, S.D.F., Hughes, P.D.M., Froese, D.G., Jensen, B.J.L., Kuehn, S.C., Mallon, G., Amesbury, M.J., Charman, D.J., Daley, T.J., Loader, N.J., Mauqouy, D., Street-Perrott, F.A., Woodman-Ralph, J., 2012. High-precision ultra-distal Holocene tephrochronology in North America. Quat. Sci. Rev. 52, 6–11.
Reimer, P.J., Bard, E., Bayliss, A., Beck, J.W., Blackwell, P.G., Bronk Ramsey, C., Grootes, P.M., Guilderson, T.P., Haflidason, H., Hajdas, I., HattŽ, C., Heaton, T.J., Hoffmann, D.L., Hogg, A.G., Hughen, K.A., Kaiser, K.F., Kromer, B., Manning, S.W., Niu, M., Reimer, R.W., Richards, D.A., Scott, E.M., Southon, J.R., Staff, R.A., Turney, C.S.M., van der Plicht, J., 2013. IntCal13 and Marine13 radiocarbon age calibration curves 0–50,000 Years cal BP. Radiocarbon 55, 4.
Robock, A., 2002. Volcanic eruptions. In: Munn, T. (Ed.), The Earth System: Physical and Chemical Dimensions of Global Environmental Change, Encyclopaedia of Global Environmental Change, vol. 1. Wiley, Chichester, pp. 738–744.
Roland, T.P., Mackay, H., Hughes, P.D.M., 2015. Tephra analysis in ombrotrophic peatlands: a geochemical comparison of acid digestion and density separation techniques. J. Quat. Sci. 30, 3–8.
Sato, H., 1971. ^{14}C age of Tarumae volcanic ash d member – ^{14}C age of the Quaternary deposits in Japan (65). Earth Sci. 25, 185–186 (in Japanese).
Sieron, K., Siebe, C., 2008. Revised stratigraphy and eruption rates of Ceboruco stratovolcano and surrounding monogenetic vents (Nayarit, Mexico) from historical documents and new radiocarbon dates. J. Volcanol. Geotherm. Res. 176, 241–264.
Sun, C., Plunkett, G., Liu, J., Zhao, H., Sigl, M., McConnell, J.R., Pilcher, J.R., Vinther, B.M., Steffensen, J.P., Hall, V.A., 2013. Ash from Changbaishan Millennium eruption recorded in Greenland ice: implications for determining the eruption's timing and impact. Geophys. Res. Lett. 41, 694–701.
Swindles, G.T., Galloway, J., Outram, Z., Turner, K., Schofield, J.E., Newton, A.J., Dugmore, A.J., Church, M.J., Watson, E.J., Batt, C., Bond, J., Edwards, K.J., Turner, V., Bashford, D., 2013. Re-deposited cryptotephra layers in Holocene peats linked to anthropogenic activity. Holocene 23, 1493e1501.
Swindles, G.T., Plunkett, G., 2011. 'The methodological basis for fine-resolution, multi-proxy reconstructions of ombrotrophic peat bog surface wetness': comments. Boreas 40, 379–381.
Tappen, C.M., Webster, J.D., Mandeville, C.W., Roderick, D., 2009. Petrology and geochemistry of ca. 2100–1000 a. B.P. magmas of Augustine volcano, Alaska, based on analysis of prehistoric pumiceous tephra. J. Volcanol. Geotherm. Res. 183, 42–62.
Tokui, Y., 1989. Volcanic Eruptions and Their Effects on Human Activity in Hokkaido, Japan after the 17th Century (Unpublished MSc. thesis). Ochanomizu University. Reproduced In: Tokui, Y. 1995. Yumi Tokui Gyoseki Syuu (Yumi Tokui Memorial Book), Ochanomizu University, pp. 111–218 (in Japanese).
Troels-Smith, J., 1955. Characterisation of unconsolidated sediments. Danmarks Geologiska Undersögelse IV. Reakke 3, 1–73.
Volynets, O.N., Ponomareva, V.V., Braitseva, O.A., Melekestsev, I.V., Chen, Ch.H., 1999. Holocene eruptive history of Ksudach volcanic massif, South Kamchatka: evolution of a large magmatic chamber. J. Volcanol. Geotherm. Res. 91, 23–42.
Wallace, B.L., 1991. L'Anse aux Meadows gateway to Vinland, the Norse of the North Atlantic. Acta Archaeol. 61, 166–197.
Wallace, B., 2003. The Norse in Newfoundland: L'Anse Aux Meadows and Vinland. Nfl Labrador Stud. 19, 5–43.
Watson, E.J., Swindles, G.T., Lawson, I.T., Savov, I.P., 2015. Spatial variability of tephra and carbon accumulation in a Holocene peatland. Quat. Sci. Rev. 124, 248–264.
Yamada, S., 1958. Studies on the history of volcanic eruptions of alluvium epoch in Hokkaido on the basis of depositional features of the pyroclastics. Monogr. Assoc. Geol. Collab. Jpn 8 (in Japanese with English abstract).
Yamaguchi, D.K., 1983. New tree-ring dates for recent eruptions of Mount St. Helens. Quat. Res. 20, 554–557.
Yamaguchi, D.K., 1985. Tree-ring evidence for a two-year interval between recent prehistoric explosive eruptions of Mount St. Helens. Geology 13, 554–557.
Yamaguchi, D.K., Hoblitt, R.P., 1995. Tree-ring dating of pre-1980 volcanic flowage deposits at Mount St. Helens Washington. Geol. Soc. Am. Bull. 107, 1077–1093.
Zielinski, G.A., Mayewski, P.A., Meeker, L.D., Whitlow, S., Twickler, M.S., Morrison, M., Meese, D., Alley, R.B., Gow, A.J., 1994. Record of volcanism since 7000 B.C. from the GISP2 Greenland ice core and implications for the volcano-climate system. Science 264, 948–952.
Zielinski, G.A., Dibb, J.E., Yang, Q., Mayewski, P.A., Germani, M.S., Whitlow, S., Twickler, M.S., 1997. Assessment of the record of the 1982 El Chichon eruption as preserved in Greenland snow. J. Geophys. Res. 102, 30045–26640.